



Relation between the energy of earthquake swarm and the Hurst exponent of random variations of the geomagnetic field

M. Hayakawa^{a,*}, K. Hattori^b, A.P. Nickolaenko^c, L.M. Rabinowicz^c

^a *The University of Electro-Communications, 1-5-1 Chofugaoka, Chofu, Tokyo 182-8585, Japan*

^b *Marine Biosystems Research Center, Chiba University, Chiba, 263-8522 Japan*

^c *Usikov Institute for Radio Physics and Electronics, Ukrainian National Academy of Sciences, Kharkov, 61085 Ukraine*

Received 6 May 2003; received in revised form 7 June 2003; accepted 10 July 2003

Available online 15 April 2004

Abstract

We present evidence that the Hurst exponent of the ultra low frequency component of the geomagnetic field varies similarly to the energy release of the local swarm of earthquakes observed in Japan in 2000. Similarity is demonstrated between the energy release by the shocks and variations of the Hurst exponent derived for the three component records of the geomagnetic field.

© 2004 Elsevier Ltd. All rights reserved.

1. Introduction

Much attention has been directed toward the search of connections between electromagnetic signals and seismic activity. A general scope of these investigations is presented in the review by Hayakawa (2001), collective monographs edited by Hayakawa and Fujinawa (1994); Hayakawa (1999); Hayakawa and Molchanov (2002). Many approaches were described in publications with a particular emphasis on detection of feasible electromagnetic (EM) precursors, i.e., the EM events preceding the earthquake (EQ) main shock. One of the well-grounded physical ideas in the field is carrying out the electromagnetic observations in the ultra-low-frequency (ULF) range, i.e., below a few Hz. Tectonic processes may cause the charge separation and electric currents flowing in the crust. These latter are able to drive electromagnetic radiation in a wide band, but only the lowest frequencies have a chance to pass through the conducting soil and reach a detector placed on the surface of the ground. Therefore, signals of seismic origin could be expected in the ULF band.

Ordinary, non-seismic, ULF signals persist permanently and are associated predominantly with the electromagnetic activity in the earth's magnetosphere; the

waveforms detected on the ground surface are known as geomagnetic pulsations. It is believed that radio signals caused by seismic and pre-seismic activity will have special features, which allow for discrimination of such signals from the customary geomagnetic activity and thus for a recognition of a hidden EQ preparatory process.

Different parameters were used in extensive long-term investigations worldwide, so that we can only mention here the most characteristic ones. The special pulsed electric signals were discovered and studied by the groups working in Greece (Varostos et al., 1994; Varostos and Lazardou, 1999; Varostos, 2001; Varostos and Sarlis, 2002). The magnetic signals driven by seismic activity were found and different parameters were investigated: the field amplitudes, gradients of different field components, the polarization, arrival direction of the disturbances, etc. (Fraser-Smith et al., 1990; Hattori et al., 2002a; Hayakawa et al., 1996; Ismaguilov et al., 2001; Kopytenko et al., 1990, 2002a; Molchanov et al., 1992; Uyeda et al., 2002). Spectra, statistical properties, and fractal characteristics of radiation of seismic origin was also studied and modeled (see, e.g., Gladyshev et al., 2002; Gotoh et al., 2002; Hobara et al., 2002; Koons et al., 2002; Smirnova, 1999; Smirnova et al., 2001; Troyan and Hayakawa, 2002; Vallianatos et al., 2002; Yagova et al., 2002; Yopez et al., 1999).

It is evident beforehand that the signals of seismic origin must have a stochastic nature like many other

* Corresponding author.

E-mail address: hayakawa@whistler.ee.uec.ac.jp (M. Hayakawa).

natural electromagnetic signals. Therefore it is not easy to even to distinguish between a emission from tectonic activity and variations in ordinary electromagnetic (EM) background. As a result, rare undeniable evidence has been presented concerning the electromagnetic phenomena associated with the earthquakes. The goal of the present paper is to demonstrate a case study of such a link found between the cumulative magnitude of the local EQ swarm and statistical properties of the ULF geomagnetic variations. The EM field records were performed at the Seikoshi observatory (34.85° N and 138.82° E, Izu Peninsula, Japan) in 2000 (see also Ismaguilov et al., 2001).

The following experimental layout was used. Three orthogonal components of the geomagnetic field were recorded. Two magnetic field sensors (Hattori et al., 2002a; Kopytenko et al., 2002a) were oriented in the plane of the geomagnetic meridian: the horizontal H -field component and the vertical, Z -component. The third sensor measured the D -field. Receiving equipment transformed the analog data into digital code with the sampling rate of $f_s = 1$ Hz. The field waveforms were stored at the hard disk of the data acquisition system (a PC computer). The monitoring was performed since 1999. Parameters of the local seismic activity were evaluated for the nearby Moshikoshi seismic station (34.88° N and 138.86° E).

2. Description of the results

The main result of the study is shown in Fig. 1. The figure includes three vertically separated plots of the records. The electromagnetic data in each frame start from February and end in December 2000. Each plot depicts the data of two sorts. The vertical bars (the same for all three frames) show the dynamics of local seismic activity indicating the time of occurrence of individual earthquakes and their magnitudes M^* measured in the units of Japan Meteorological Agency (JMA). The swarm of earthquakes is clearly seen starting at the end of June 2000. The earthquakes were included, which occurred within the 100 km zone centered at the Moshikoshi seismic station (34.88° N and 138.86° E). Since this station is approximately 5 km away from the Seikoshi observatory (34.85° N and 138.82° E) where the electromagnetic records were performed, we accept that the local seismic activity is evaluated for the 100 km circle centered at the geomagnetic observatory.

The solid lines in Fig. 1 show variations of the basic principal component found in the Hurst exponents (see Appendixes A and B) derived for the random ULF variations in the H , D , and Z - fields correspondingly. A few ‘zero level’ horizontal sections of the records of the Hurst exponent correspond to the intervals when the data were not collected owing to technical reasons

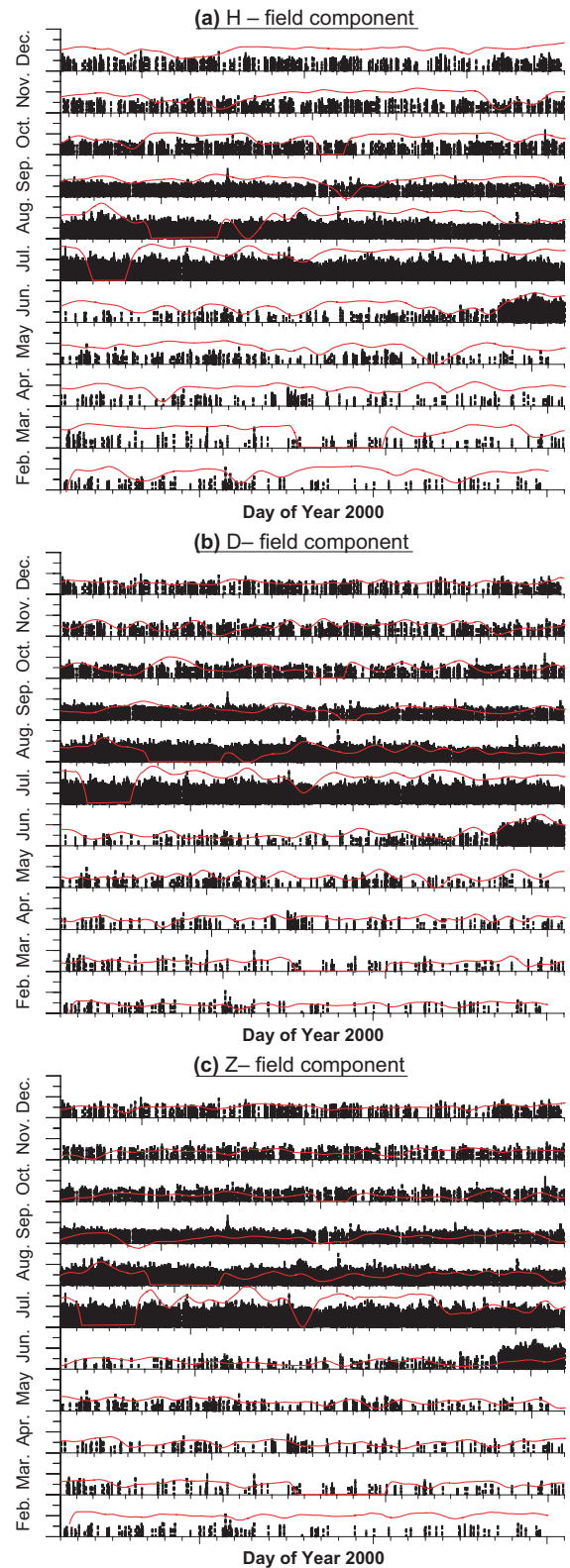


Fig. 1. Variations of the local seismic activity (vertical bars) and the main principal component of the Hurst exponent derived for ULF fluctuations of the geomagnetic field (red lines). Vertical bars indicate times of occurrence and JMA magnitude of EQ. The swarm of EQ started on June 26th. Horizontal geomagnetic field components vary coherently with the seismicity.

(mainly the service and maintenance of the equipment).

One may observe from Fig. 1 that a swarm of the earthquakes starts around June 26th–27th: a substantial increase in both the rate and in the magnitude of individual shocks is seen there. Seismic activity remained high for about three months, and afterwards it gradually returned to the usual level. The plots in Fig. 1 demonstrate that the Hurst exponent, which reflects the statistical properties of the random component of the

geomagnetic field, vary consistently with the local seismic activity. Similarity is especially noticeable for the horizontal components *H* and *D* while the vertical component *Z* does not show such a clear alterations.

A few words should be said explaining why we select the Hurst exponent for investigation. Much effort was already directed to the detection of ULF radio signals connected with the seismic activity, but the outcome remains ambiguous. From the other hand, one may expect that seismic and pre-seismic electromagnetic

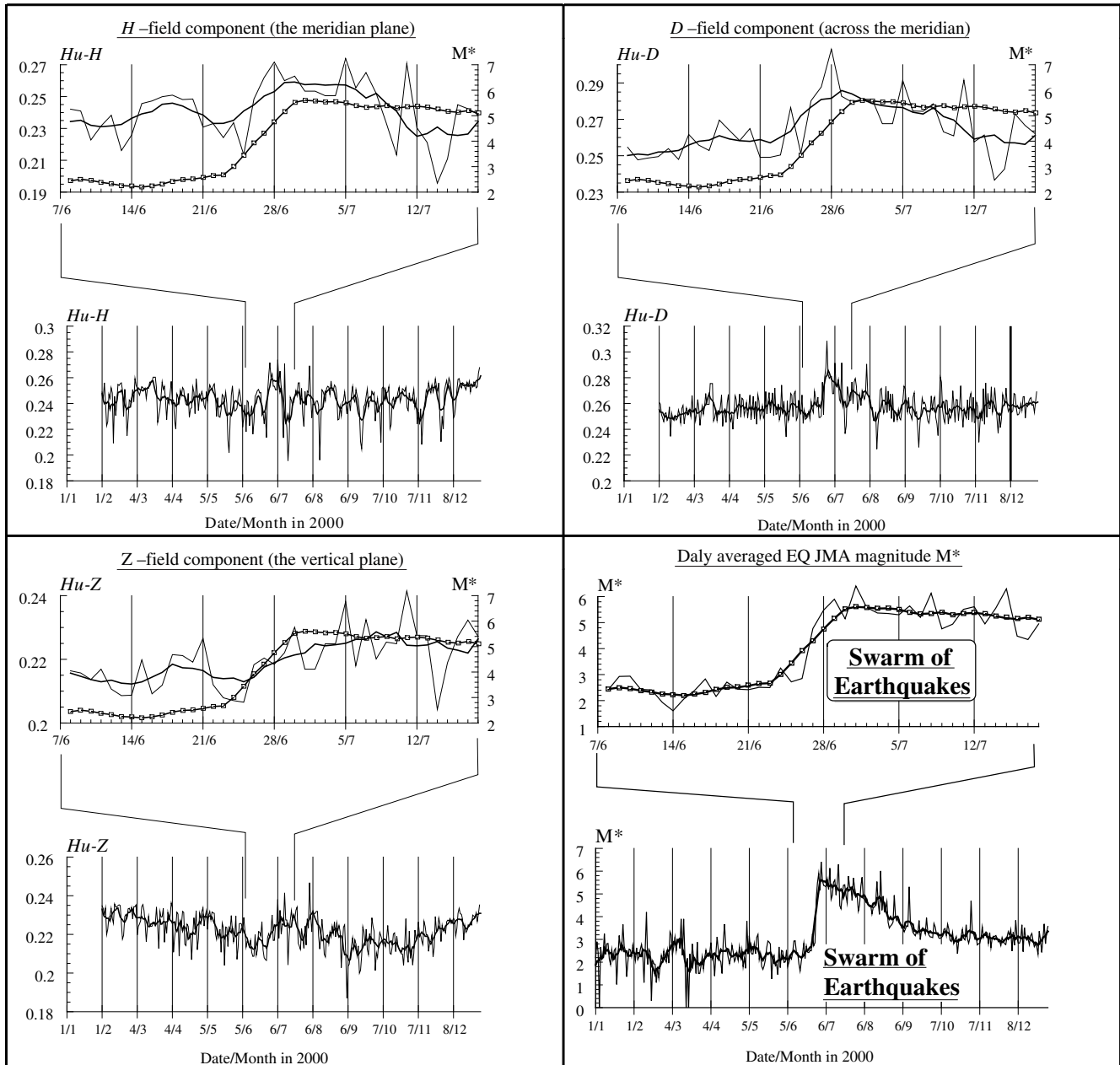


Fig. 2. Variations of the Hurst exponent derived for the geomagnetic field ULF fluctuations. The local seismic activity is shown by the bottom right frame. Lower plots in each frame depict annual variations day by day. Thin lines correspond to the diurnal resolution and the thick smooth lines show the running average of the data with the window of ± 3 days width. The upper plots in each pair extend the interval around the onset of the earthquake swarm. Solid line with open squares depicts ± 3 days running average of the daily magnitude of the earthquakes.

activity must result in specific signals. The key problem, as we noted above, is the distinguishing of such signals from the bulk of ordinary ULF background. The customary signals connected with the geomagnetic activity, such as periodic pulsations and radiation from the thunderstorms, the signals originating from the industrial activity, and the signals induced by mechanical vibrations of the field sensors in the outer geomagnetic field form this background. We have chosen the Hurst exponent as the characteristic responsive to the internal statistical properties of the record and simultaneously insensitive toward the amplitude of the signal.

As we show in Appendix A, the Hurst exponent is found from the ratio of the range of a random series (i.e., the maximum minus its minimum value) to the standard deviation of the same variable. Therefore, the Hurst exponent is independent of the amplitude. For example, suppose we have a record of variable amplitude, or the gain of equipment abruptly varies. Such variations will have no impact on the Hurst exponent unless the statistical properties of the record remain invariant. One may expect that a radio signal originating from the seismic activity has the statistical properties that do not coincide with the above mentioned processes, so that presence of a novel component will be immediately detected by the Hurst exponent.

Fig. 1 is the annual survey of temporal variations, therefore, only the general behavior could be grasped from here. Variations in more detail are shown in Fig. 2 where we plot the vicinity of the onset of the earthquake swarm. Four pair plots are shown. Three of them correspond to the Hurst exponents derived for individual geomagnetic field components and the fourth frame depicts the daily averaged earthquake magnitude. The quantity characterizes the energy release by the local earthquakes.

Shown in Fig. 2 are the Hurst exponents found for individual geomagnetic field components H , D , and Z . The lower plot in each pair surveys the annual variations. The date (UT) is depicted on the abscissa with the 31-day step, and the Hurst exponent is plotted on the left ordinate. The thin lines in each frame show the daily averaged data, and the thick lines depict the running average with the window of ± 3 days width.

The upper plot in each pair separately depicts the interval 41 day long centered at the onset of the swarm. Date is shown on the abscissa with the one-week step, the Hurst exponent is plotted on the left ordinate. Additional curve marked with open squares presents the concurrent ± 3 days running average of the JMA earthquake magnitude M^* plotted on the right ordinate.

The lower right frame in Fig. 2 demonstrates dynamics of the local seismic activity in the same manner. Plots of Fig. 2 allow us to conclude that variations have similar patterns. Local seismic activity and the Hurst exponents derived for horizontal components of the

geomagnetic field vary more coherently, while variations in the vertical field component are not so pronounced.

3. Discussion

We demonstrated existence of similarity between temporal variations of the Hurst exponent and the power release of the local earthquakes. Allied variations of these two characteristics are clearly seen in the data around the onset of the swarm of the earthquakes. A clear response was observed when the swarm started, and connections decrease afterwards, as if some kind of ‘saturation’ takes place. Therefore, the Hurst exponents and the earthquake energy release do not vary jointly all the time (see Fig. 2). Simultaneously, such a behavior indicates that the signal detected in the Hurst exponent hardly can be attributed to mechanical trembling of the soil and field sensors: the swarm continues and the antennas vibrate, but the cross-correlation between the two processes is diminishing. We must have in mind also that all three antennas vibrate coherently, while the Hurst exponents of individual field components vary in different ways. These considerations allow us to exclude the trembling of antennas from possible mechanisms responsible for the effects observed.

The driving idea we used in the study was of a traditional kind: the seismic activity might add a signal into the ULF record. Statistical properties of the seismic radio signals should be different from those pertinent to ordinary terrestrial electromagnetic activity, say, to the emissions from the magnetosphere or to the radiation from the global thunderstorm activity. To detect additional signal, a novel approach was applied.

The first novelty is that we apply the R/S analysis to the recorded geomagnetic data and derive the relevant Hurst exponents for the series collected in the seismically active region. Since the Hurst exponent depends on the internal structure of the random or chaotic signal, we expect that presence of the seismogenic ULF radio emission will be revealed as an alteration of the statistics: that the Hurst exponent will diverge from that of ordinary ULF records made in quiet conditions.

The second novelty is that we apply the principal component analysis (PCA) when extracting the regular trends from the temporal variations of the Hurst exponents. Applications of such a procedure is conditioned by two features of the signal:

1. The initial (raw) temporal variations of the Hurst exponent are noisy, and an additional processing must be included to obtain more regular variations.
2. The important advantage of the PCA procedure is that it expands a time series over an orthogonal basis, and the basis itself is constructed from the time series.

We have to mention also the applications of the R/S analysis and of the Hurst exponent is becoming a common tool in geophysical research (see, e.g., Turcotte, 1997; Nickolaenko et al., 2000; Nickolaenko and Hayakawa, 2002). It suggests an effective and simple way for evaluating the properties of radio noise. From the other hand, the PCA analysis (Danilov and Zhiglyavsky, 1997; Troyan and Hayakawa, 2002) could be considered as a further development of well-known algorithms of spectral processing (see, e.g., Marple, 1987).

4. Conclusion

The authors of this study see their major goal in driving the attention of the scientific community to the detection of the link between the earthquake swarm power release and the statistical properties of the geomagnetic ULF radio signal. We tried to describe the measurement and processing of the signal in every detail. We hope that similar processing of independent series of data will be carried out or separate measurements will be performed, which confirm our results and conclusions.

Experimental investigation of the long-term records of the ULF geomagnetic data in the seismically active region indicates that the Hurst exponents pertinent to random field variations varies in accord with the earthquake energy release. Similarity of the variations testifies that regional seismic energy release is connected with the statistical properties of EM noise, which modifies the ULF geomagnetic record.

Further investigations are desirable that will provide us with

- an extended set of experimental data connecting the energy release of several earthquake swarms and the statistical properties of the ULF geomagnetic signal,
- improve the time resolution aiming on establishing the character of variations in the ULF field (the precursor or a successor).

Appendix A. Fundamentals of the R/S analysis

The R/S analysis and the Hurst exponent characterize the internal structure of a noise indicating on the links, which dominate in the stochastic signals (Turcotte, 1997). In the present work, we apply the modified R/S analysis to study the properties of fluctuations present in the geomagnetic field.

The accumulated data set is relatively big since the sampling rate is 1 Hz. Data sets continue typically for the periods of about 30 days with short interruptions for service, calibration, copying the accumulated data files, maintenance of the equipment etc., which may reach sometimes a few days. Plots we show in Fig. 3 display a fragment of the data covering about half an hour. The

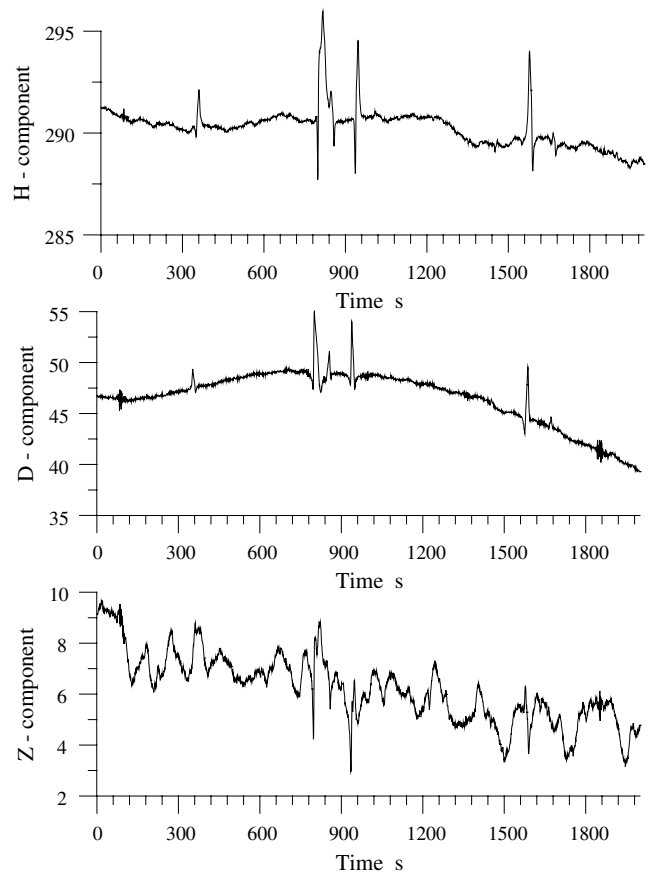


Fig. 3. Sample record of the Seikoshi ULF signal recorded at the beginning of August 08, 2000.

UT is shown on the abscissa counted in seconds from the beginning of August 08, 2000. The amplitude of the geomagnetic field components is depicted along the ordinate in arbitrary units. The upper plot shows the horizontal H -component that is the largest one. The middle plot depicts variations of the orthogonal horizontal field component D , and the lower plot demonstrates evolution of the vertical component Z of the geomagnetic field. As a whole, the records contain diurnal patterns (not shown) and the irregular pulsed fluctuations. These pulses are relatively rare, they occur at a rate about one pulse per 100 s, their amplitude may be high, and the pulses might be connected with the local industrial activity.

The objective of our study is the fast fluctuation component of the signal, which is caused by random deviations of the field from the regular daily pattern. The Hurst exponent (H_u) is obtained in the R/S analysis of random data (Turcotte, 1997). The standard R/S procedure is performed in the following way. Suppose we have a series of random data $x(t_K) = x_K$, where $K \in [1, N]$, and that the following binary condition is satisfied for convenience $N = 2^L$. We divide the initial series x_K in two halves containing $M = N/2$ samples and find two ranges of the variable $R_M = x_{\text{MAX}} - x_{\text{MIN}}$

pertinent to each sub-interval and of the standard deviations $S_M = \sqrt{\frac{1}{M-1} \sum_{K=1}^M (y_K - \langle y_M \rangle)^2}$ of a supplementary process y_K which is the following sum $y_K = \sum_{i=0}^K x_i$. Angular brackets denote the averaging over the ensemble. After obtaining the R_M and S_M quantities, we compute and the average ratio:

$$Z_M = Z(N/2) = \langle R_M/S_M \rangle \tag{A.1}$$

The ratio found is plotted in the form $\log_2(Z_M)$ against the argument $I = \log_2(M)$, see the diagram in Table 1. This is the extreme right point (1) in the R/S curve. As the next step, we divide the data into four parts (see Table 1) and repeat the procedure by calculating the new ratio $Z_M = Z(N/4)$ thus obtaining the second point (2) in the R/S plot shown in Table 1. The procedure is repeated for decreasing duration: $M = N/8, M = N/16$, and so on. Finally, when $M = 2$, the elementary segment of data contains only two quantities, and the parameters R and S satisfy the obvious condition $R_2 = \sqrt{2} \cdot S_2$. So, the initial value of the R/S ratio is a constant

$$Z_2 = \langle R_2/S_2 \rangle = \text{const} = \sqrt{2} \tag{A.2}$$

We modify the standard R/S algorithm in the present study: the same x_K succession is used without summation procedure when obtaining the standard deviation.

It is clear that all the plots R/S versus I start from the same point $\log_2 \sqrt{2} = 0.5$ when $M = 2$, as Table 1 shows. We depict in this table the results of real processing of a segment of the H -field component record 128 s long.

Relations above indicate an important property of the R/S ratio, and hence, of the Hurst exponent: an ‘automatic’ normalization of the data takes place in the course of processing. As a result, both the ratio and the exponent do not depend on the amplitude of the signal, they depend on the internal structure of the noise. This also means that events like changing the gain in the process of data collecting have minor impact on the results of R/S procedure, which is very important in processing of real data.

The Hurst exponent is found from the power law

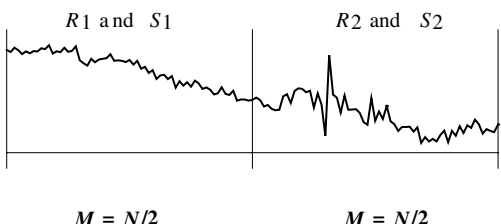
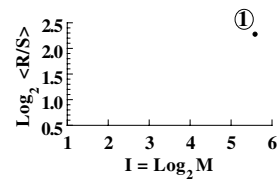
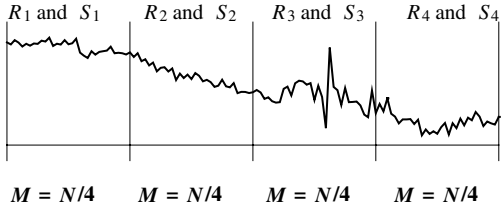
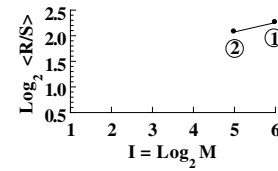
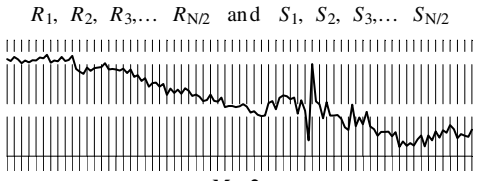
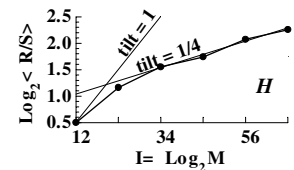
$$Z_M = (M)^{Hu} \tag{A.3}$$

so that the tilt of the best fit straight line gives the value of the Hurst exponent, as is shown in Table 1. It is easy to see that the current value of $Hu(I)$ is equal to:

$$Hu(I) = \log_2(Z_{M+1}) - \log_2(Z_M) \tag{A.4}$$

The slope of classical and modified R/S curves varies with the length of data segment: when I is small, the Hurst exponent is close to unity, and it decreases when I

Table 1
Diagram of the R/S procedure

Signal partition	Values obtained	R/S plot
 <p style="text-align: center;">$M = N/2$ $M = N/2$</p>	$Z_2 = Z(N/2) = \langle R/S \rangle_2$	
 <p style="text-align: center;">$M = N/4$ $M = N/4$ $M = N/4$ $M = N/4$</p>	$Z_4 = Z(N/4) = \langle R/S \rangle_4$	
etc., until $M = 2$		
 <p style="text-align: center;">$M = 2$</p>	$M = 2 ;$ $Z_{N/2}(2) = \sqrt{2}$	

grows. For example, when we treat the Gaussian white noise, the tilt of the short samples is characterized by $Hu \rightarrow 1$. It decreases to $Hu = 0.5$ stationary value when the length of the segments M becomes large enough and we use the classical R/S analysis (Rytov, 1976; Turcotte, 1997). In our case of modified R/S procedure, the stationary tilt is reduced, and the ‘knee area’ between the stationary and non-stationary areas of the plot becomes more pronounced. We exploit this feature in a hope that it makes the modified Hurst exponent more sensitive toward any modifications in the nature of signal processed.

To sustain relatively high time resolution, we used in the R/S processing the standard duration of the data set that is equal to 128 s. As a result, the R/S curves were obtained the 128 s step. Relevant Hurst exponents were found as $Hu(3) = \log_2(Z_3) - \log_2(Z_4)$ for each field component. As one may see from Table 1, the level chosen corresponds to the curve of already ‘stable’ ≈ 0.25 tilt. The results obtained do not substantially vary when we choose any other level I .

Appendix B. Principal component analysis

We obtain the Hurst exponents as the functions of time as a result of the processing. The curves presenting temporal dependence have regular variations hidden in the noise. Since our objective are the regular variations, we have to extract them from the noise, and we apply for this purpose the the principal component analysis (PCA), namely the ‘Caterpillar’ algorithm (Danilov and Zhiglyavsky, 1997; Troyan and Hayakawa, 2002). The PCA algorithms are described in literature, therefore we note here the main points of the procedure. We have to note that PCA is a recent development of advanced processing algorithms such as MUSIC (multiple signal classification) and EV (eigenvector) procedure (Marple, 1987). From the physical point of view, the PCA provides the results which are similar to the signal filtering, the distinction is that the response functions are constructed automatically right from the input data.

The Caterpillar algorithm of the principal component analysis is performed in the following way (Danilov and Zhiglyavsky, 1997). Let us assume that we have a finite time series $x(t_k) = x_k$ with $1 \leq k \leq N$. We choose an integer number $L < N$ regarded as the ‘caterpillar’ length and transform the initial one–dimension data set x_k into the two-dimension matrix. The first L points of the original series (we use $L = 120$ in the present work) are placed in the first row of the matrix. Elements from x_2 to x_{L+1} are placed in the second line, etc. The process continues until we reach the end of the data set. The last line of the matrix contains the elements with indices starting from $k = (N - L + 1)$, so that here we find

the last L samples of the series, namely, $x_{N-L+1}, x_{N-L+2}, \dots, x_N$.

As the second step of the PCA processing, we construct the eigen-values and the eigen-vectors of the above matrix. It is clear that these parameters depend on the structure of the signal $x(t_k)$ and simultaneously they allow us to construct the ‘internal basis’: the principal components. This stage of the procedure is equivalent to generating the bank of linear filters, and each of these filters is tuned to a single principal component of the signal (Danilov and Zhiglyavsky, 1997).

At the third step, we visualize, survey, and select the desired principal components discovered in the record at the previous step. In our particular case, we take the components having the slowest variations (principal component 1).

The final, fourth step implies the reconstruction of the signal by extracting and combining the selected principal components of the signal. This step is similar to choosing a set of desired harmonics in the customary Fourier transform.

The PCA procedure turns into an ordinary Fourier transform when the initial succession is an infinite sinusoidal signal. In this case, the matrix constructs the sine and cosine basic functions, and the result coincides with the well-known procedures (Danilov and Zhiglyavsky, 1997).

To illustrate how the principal component analysis works, we process a segment of the modified Hurst exponent derived for D -component of the geomagnetic field. The initial $Hu - D(t)$ data are given by the upper plot in Fig. 4 labeled ‘Raw Data’. The abscissa shows time (UT) with the step of 128 s for the interval from June 20 to June 30, 2000. The Hurst exponent of the D -geomagnetic field is plotted on the ordinate.

The labels on the ordinate correspond to the ‘running average’ line, so that the Hurst exponent $Hu - D$ varies around 0.269 median value. The running average line corresponds to the data averaged over ± 21 points (approximately over an hour interval). All other plots were shifted vertically (the vertical scale was preserved) to facilitate their comparison. The irregular ‘Raw Data’

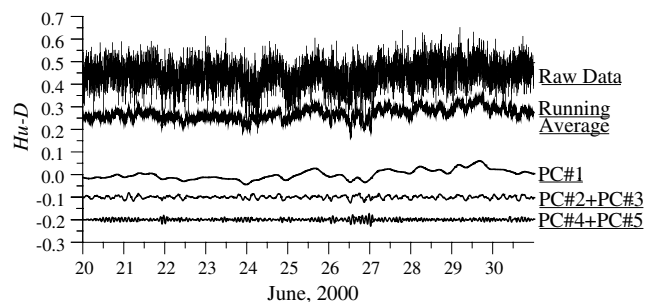


Fig. 4. Temporal variations and principal components of the Hurst exponent of D -field during the last decade of June, 2000.

line was shifted upward. Three lines shifted downward from the running average line depict variations of principal components (PC) found by the PCA ‘Caterpillar’ procedure. It is easy to see that time series of the basic principal component (PC#1) might be regarded as ‘a well averaged day after day trend’, as the comparison with the running average shows.

Plots in Fig. 4 illustrate how the PCA procedure separates the trend and periodic variations hidden in initial ‘Raw Data’ record. The principal components corresponding to periodic variations are usually extracted as pairs, for example, in the particular case shown in Fig. 4 the following components are coupled: PC2 + PC3, PC4 + PC5, etc. Decomposition into pairs is easily explained. Each pair contains mutually orthogonal ‘sine’ and ‘cosine’ sub-signals of the same frequency: their Lissajous figures have the circular form. The latter property is used when choosing the pair of principal components for signal reconstruction. Thus, the typical decomposition (reconstruction) of a signal with the PCA algorithm has the form: PC1 being the trend, which is close to the running average, and the periodic components PC2 + PC3, PC4 + PC5, etc. When slow trends are absent in the initial succession, only periodical components remain of an altered numeration PC1 + PC2, PC3 + PC4, etc.

We may compare the PC#1 plot of Fig. 4 with the lines shown in Figs. 1 and 2 and notice slight deviations between these graphs. This is not surprising since we use for illustration in Fig. 4 only a short section of the continuous record 10 days long. The complete data set is processed for obtaining Figs. 1 and 2 contained 37 days, and we know that changing of the initial data set might alter the basis vectors constructed by the PCA algorithm. So, the illustrative plots of Fig. 4 experienced a slight modification in comparison with the complete data set. Still, the overall growth in the Hurst exponent of 0.04 is present in Fig. 4, which also starts at a right time: from June 27th.

Concluding, we must note that applications of the PCA algorithms allowed us to single out the trends present in the statistical characteristics of the geomagnetic noise. Simultaneously, we must have in mind an important property of the algorithm: the results of processing are sensitive to the length of time series and to presence of gaps in the data. This property is pertinent to all ‘spectral’ algorithms, including the ordinary Fourier transform, method of maximum entropy, different kinds of filtering, etc. Therefore, the data series we process to obtain the trends must be accurate and contain no gaps.

Two lower curves in Fig. 4 demonstrate the results of the signal reconstruction when we pick the sums of the most intense principal components PC#2 + PC#3 and PC#4 + PC#5. The ‘Caterpillar’ software evaluates the distribution of the signal energy over the principal

components: the PC#1 carries 17.6% of the intensity and PC#2, PC#3, PC#4 and PC#5 correspond to 2.3%, 1.4%, 1.2%, and 1.2% shares. Higher frequency having the period between 2 and 3 h is always present in the $Hu(t)$ dependence, in our case it is introduced by the PC#4 + PC#5 combination. The origin of such periodic variations is not clear yet: it might reflect the stochastic processes in the earth interior or it could be associated with the random variations in the solar wind that interacts with the terrestrial magnetic field.

References

- Danilov, D.L., Zhiglyavsky, A.A. (Eds.), 1997. Principal Component of the Time Series: The Caterpillar Method. St.-Petersburg state University, St.-Petersburg, Russia, p. 307 (in Russian).
- Fraser-Smith, A.C., Bernardy, A., McGill, P.R., Ladd, M.E., Helliwell, R.A., Villard Jr., O.G., 1990. Low frequency magnetic field measurements near the epicenter of the Loma-Prieta earthquake. *Geophys. Res. Lett.* 17, 1465–1468.
- Gladyshev, V., Baransky, L., Schekotov, A., Fedorov, E., Pokhotelov, O., Andreevsky, S., Rozhnoi, A., Khabazin, Y., Belyaev, G., Gorbatiykov, A., Gordeev, E., Chebrov, V., Sinitin, V., Lutikov, A., Yunga, S., Kosarev, G., Surkov, V., Molchanov, O., Hayakawa, M., Uyeda, S., Nagao, T., Hattori, K., Noda, Y., 2002. Some preliminary results of seismo-electromagnetic research at complex geophysical observatory, Kamchatka. In: Hayakawa, M., Molchanov, O.A. (Eds.), *Seismo Electromagnetics: Lithosphere–Atmosphere–Ionosphere Coupling*. TERRAPUB, Tokyo, pp. 421–432.
- Gotoh, K., Akinaga, Y., Hayakawa, M., Hattori, K., 2002. Principal component analysis of ULF geomagnetic data for Izu islands earthquakes in July 2000. *J. Atmos. Electricity* 22 (1), 7–15.
- Hattori, K., Askinaga, Y., Hayakawa, M., Yumoto, K., Nagao, T., Uyeda, S., 2002a. ULF magnetic anomaly preceding the 1997 Kagoshima earthquakes. In: Hayakawa, M., Molchanov, O.A. (Eds.), *Seismo Electromagnetics: Lithosphere–Atmosphere–Ionosphere Coupling*. TERRAPUB, Tokyo, pp. 19–29.
- Hattori, K., Takahashi, I., Yoshino, C., Nagao, T., Liu, J.I., Shieh, C.F., 2002b. ULF geomagnetic and geopotential Measurements at Chia-Yi, Taiwan. *J. Atmos. Electricity* 22 (3), 217–222.
- Hayakawa, M., Kawate, R., Molchanov, O.A., Yumoto, K., 1996. Results of ultra-low-frequency magnetic field measurements during the Guam earthquake of August 08, 1993. *Geophys. Res. Lett.* 23, 241–244.
- Hayakawa, M., Fujinawa, Y. (Eds.), 1994. *Electromagnetic Phenomena Related to Earthquake Prediction*. TERRAPUB, Tokyo, p. 677.
- Hayakawa, M. (Ed.), 1999. *Atmospheric and Ionospheric Electromagnetic Phenomena Associated with Earthquakes*. TERRAPUB, Tokyo, p. 996.
- Hayakawa, M., 2001. Electromagnetic phenomena associated with earthquakes: Review. *Trans. IEE of Japan* 121A (10), 893–898.
- Hayakawa, M., Molchanov, O.A., 2002. *Seismo electromagnetics: Lithosphere–Atmosphere–Ionosphere Coupling*. TERRAPUB, Tokyo, p. 477.
- Hobara, Y., Koons, H.C., Roeder, J.L., Yamaguchi, H., Hayakawa, M., 2002. New ULF/ELF observation in Seikoshi, Izu, Japan and the precursory signal in relation with large seismic events at Izu Islands in 2000. In: Hayakawa, M., Molchanov, O.A. (Eds.), *Seismo Electromagnetics: Lithosphere–Atmosphere–Ionosphere Coupling*. TERRAPUB, Tokyo, pp. 41–44.
- Ismaguilov, V.S., Kopytenko, Yu., Hattori, K., Voronov, P.M., Molchanov, O.A., Hayakawa, M., 2001. ULF magnetic emission

- connected with under sea bottom earthquakes. *Natural Hazards and Earth System Sciences* 1, 23–31.
- Koons, H.C., Roeder, J.L., Hobar, Y., Hayakawa, M., Fraser-Smith, A.C., 2002. Statistical analysis of the data from the ULF sensors at Seikoshi station. In: Hayakawa, M., Molchanov, O.A. (Eds.), *Seismo Electromagnetics: Lithosphere–Atmosphere–Ionosphere Coupling*. TERRAPUB, Tokyo, pp. 29–39.
- Kopytenko, Yu.A., Matiashvili, T.G., Voronov, P.M., Kopytenko, E.A., Molchanov, O.A., 1990. Discovering of ultra-low-frequency emissions connected with Spitak earthquake and its aftershock activity in data of geomagnetic pulsation observations at Dusheti and Vardzija. *IZMIRAN, Moscow, Preprint No. 3 (888)* 27 pp.
- Kopytenko, Yu.A., Ismagilov, V.S., Hattori, K., Voronov, P.M., Hayakawa, M., Molchanov, O.A., Kopytenko, E.A., Zaitsev, D.D., 2002a. Monitoring of the ULF electromagnetic disturbances at the station network before EQ in seismic zones of Izu and Chiba peninsulas (Japan). In: Hayakawa, M., Molchanov, O.A. (Eds.), *Seismo Electromagnetics: Lithosphere–Atmosphere–Ionosphere Coupling*. TERRAPUB, Tokyo, pp. 11–18.
- Kopytenko, Yu.A., Ismagilov, V.S., Molchanov, O.A., Kopytenko, E.A., Voronov, P.M., Hattori, K., Hayakawa, M., Zaitsev, D.D., 2002b. Investigation of ULF magnetic disturbances in Japan during seismic active period. *J. Atmos. Electricity* 22 (3), 207–215.
- Marple Jr., S.L., 1987. *Digital Spectral Analyses with Applications*. Prentice-Hall, Englewood Cliffs, New Jersey. p. 345.
- Molchanov, O.A., Kopytenko, Yu.A., Voronov, P.M., Kopytenko, E.A., Matiashvili, T.G., Fraser-Smith, A.C., Bernardi, A., 1992. Results of ULF magnetic field measurements near the epicenters of the Spitak ($M_s = 6.9$) and Loma-Prieta ($M_s = 7.1$) earthquakes. *Geophys. Res. Lett.* 19, 1495–1498.
- Nickolaenko, A.P., Price, C., Iudin, D.D., 2000. Hurst exponent derived for natural terrestrial radio noise in Schumann resonance band. *Geophys. Res. Lett.* 27, 3185–3188.
- Nickolaenko, A.P., Hayakawa, M., 2002. *Resonances in the Earth-ionosphere cavity*. Kluwer Academic Publishers, Dordrecht–Boston–London. p. 380.
- Rytov, S.M., 1976. *Introduction to Statistical Radio Physics, Part 1: Random Processes*. Moscow, Nauka, 1976, pp. 204–210 (in Russian).
- Smirnova, N., 1999. The peculiarities of ground-observed geomagnetic pulsations as the background for detection of ULF emissions of seismic origin. In: Hayakawa, M. (Ed.), *Atmospheric and Ionospheric Electromagnetic Phenomena Associated with Earthquakes*. TERRAPUB, Tokyo, pp. 215–232.
- Smirnova, N., Hayakawa, M., Gotoh, K., Volobuev, D., 2001. Scaling characteristics of ULF geomagnetic fields at the Guam seismoactive area and their dynamics in relation to the earthquake. *Natural Hazards and Earth System Sciences* 1, 119–126.
- Troyan, V.N., Hayakawa, M., 2002. Methods for geophysical processing in seismic active zones. In: Hayakawa, M., Molchanov, O.A. (Eds.), *Seismo Electromagnetics: Lithosphere–Atmosphere–Ionosphere Coupling*. TERRAPUB, Tokyo, pp. 215–221.
- Turcotte, D.L., 1997. *Fractals and Chaos in Geology and Geophysics*, Second ed. Cambridge University Press, Cambridge. pp. 1159–1162.
- Uyeda, S., Nagao, T., Hattori, K., Noda, Y., Hayakawa, M., Miyaki, K., Molchanov, O.A., Gladyshev, V., Baransky, L., Schekotov, A., Belyaev, G., Fedorov, E., Pokhotelov, O., Andreevsky, S., Rozhnoi, A., Khabazin, Y., Gorbatiy, A., Gordeev, E., Chebrov, V., Lutikov, A., Yunga, S., Kosarev, G., Surkov, V., 2002. Russian–Japanese complex geophysical observatory in Kamchatka for monitoring of phenomena connected with seismic activity. In: Hayakawa, M., Molchanov, O.A. (Eds.), *Seismo Electromagnetics: Lithosphere–Atmosphere–Ionosphere Coupling*. TERRAPUB, Tokyo, pp. 413–419.
- Vallianatos, F., Lapenna, V., Troyan, V., Smirnova, N., Kopytenko, Y., Korepanov, V., Matiashvili, T., 2002. Study of the ULF electromagnetic phenomena related to earthquakes: strategy of SUPRE project. In: Hayakawa, M., Molchanov, O.A. (Eds.), *Seismo Electromagnetics: Lithosphere–Atmosphere–Ionosphere Coupling*. TERRAPUB, Tokyo, pp. 437–442.
- Varostos, P., Ueda, S., Alexopoulos, K., Nagao, T., Lazaridou, M., 1994. Prediction of recent destructive seismic activities in Greece based on seismic electric signals. In: Hayakawa, M., Fujinawa, Y. (Eds.), *Electromagnetic Phenomena Related to Earthquake Prediction*. TERRAPUB, Tokyo, pp. 13–25.
- Varostos, P., Lazardou, M., 1999. A review of the VAN method. In: Hayakawa, M. (Ed.), *Atmospheric and Ionospheric Electromagnetic Phenomena Associated with Earthquakes*. TERRAPUB, Tokyo, pp. 47–53.
- Varostos, P., 2001. A review and analysis of electromagnetic precursory phenomena. *Acta Geophys.* Pol. 49, 1–42.
- Varostos, P., Sarlis, N., 2002. A review of recent VAN efforts: the explanations of SES physical properties. In: Hayakawa, M., Molchanov, O.A. (Eds.), *Seismo Electromagnetics: Lithosphere–Atmosphere–Ionosphere Coupling*. TERRAPUB, Tokyo, pp. 131–140.
- Yagova, N., Yumoto, K., Pilipenko, V., Hattori, K., Nagao, T., Saita, K., 2002. Local variations of geomagnetic ULF noises and their relation to seismic activity. In: Hayakawa, M., Molchanov, O.A. (Eds.), *Seismo Electromagnetics: Lithosphere–Atmosphere–Ionosphere Coupling*. TERRAPUB, Tokyo, pp. 45–48.
- Yepez, E., Pineda, J.G., Peralta, J.A., Porta, A.V., Pavia-Miller, C.G., Angulo-Braun, F., 1999. Spectral analysis of ULF electric signals possible associated to Earthquakes. In: Hayakawa, M. (Ed.), *Atmospheric and Ionospheric Electromagnetic Phenomena Associated with Earthquakes*. TERRAPUB, Tokyo, pp. 115–125.